International Journal of Lightweight Materials and Manufacture 6 (2023) 285–295

Contents lists available at ScienceDirect

International Journal of Lightweight Materials and Manufacture

journal homepage: www.keaipublishing.com/ijlmm

Original Article

Influence of post-processing CO_2 laser cutting and FFF 3D printing parameters on the surface morphology of PLAs: Statistical modelling and RSM optimisation

M. Karamimoghadam [a], M. Lalegani Dezaki [b], A. Zolfagharian [c], M. Bodaghi [b, *]

[a] Department of Mechanics, Mathematics and Management, Polytechnic University of Bari, Via Orabona 4, 70125 Bari, Italy
[b] Department of Engineering, School of Science and Technology, Nottingham Trent University, Nottingham, NG11 8NS, UK
[c] School of Engineering, Deakin University, Geelong, VIC 3216, Australia

ARTICLE INFO

Article history:
Received 18 December 2022
Received in revised form
10 January 2023
Accepted 30 January 2023
Available online 4 February 2023

Keywords:
3D printing
Post-processing
Laser cutting
Fused filament fabrication
Polymers
Response surface method

ABSTRACT

This study investigates the optimization of 3D printing and CO_2 laser cutting parameters by the design of experiments (DOE) and response surface methodology (RSM). In fused filament fabrication (FFF) process, the surface quality of printed curves is poor due to the stairstep defects. The aim is to determine how the laser cutting parameters affect the surface morphology of surface finishing polylactic acid (PLA) samples. A total of 13 cube shape samples are 3D-printed with a cone-shaped hole in the middle. Then, post-processing CO_2 laser cutting with a maximum power of 1 kW is used to cut the 3D-printed products. Infill percentage (IP) and extruder temperature (ET) in 3D printing, and laser power (LP), scanning speed (SS), and top edge in CO_2 laser cutting are the main parameters in this study. Regression equations are obtained by doing an analysis of the experimental findings using statistical software to examine the impacts of process factors on surface conditions. Results show that the infill percentage and extruder temperature have an extraordinary effect on 3D-printed products' surface quality. 30% infill percentage and 190 °C extruder temperature result in the lowest surface quality with a value of 2.151 μm using DOE and RSM optimization. Also, the lowest value of the top edge is achieved at 275 μm with 300 W laser power and a 5 mm/s cutting speed. The proposed methods can be used to reduce material consumption in the product development.

1. Introduction

Among 3D printing technologies, fused filament fabrication (FFF) is a low-cost technology with high capability in building decentralized products [1–4]. Complex features and precise details which have been difficult to produce with conventional technologies are now made layer by layer without human interaction easily. This machinery is a handy tool in making thermoplastic, composite, and even metallic components [5–7]. 3D-printed products are built layer by layer from bottom to top by assigning the proper parameters, which have a high impact on the final quality. The molten layer is deposited and cooled at room temperature by following the generated G-code. The machine follows the assigned path to complete the printing procedure. Build orientation, infill pattern/density, extruder temperature, and layer thickness are the most vital ones that need to be optimized in the FFF process [8]. Despite its potential in making various products for different industrial sectors, limitations such as shrinkage, rough surface, and poor geometrical accuracy due to the stairstep effects and support structure still exist [9]. Thus, post-processing technologies and hybrid manufacturing can be used as alternative/secondary processes to eliminate these obstacles [10,11]. These processes are divided into mechanical and chemical treatment finishing, such as machining, laser cutting, sandblasting, painting, electroplating, and vapor smoothing [12].

Although mechanical properties and surface integrity are always critical, the appropriate secondary manufacturing procedure for FFF products should also be considered. Laser cutting is the most modern technology for joining or cutting films, sheets, semi-rigid,

* Corresponding author.
E-mail address: mahdi.bodaghi@ntu.ac.uk (M. Bodaghi).
Peer review under responsibility of Editorial Board of International Journal of Lightweight Materials and Manufacture.

https://doi.org/10.1016/j.ijlmm.2023.01.004

and rigid plastic components by targeting them with a concentrated laser [13]. The advantages of the laser-based process over other post-processing techniques include: no interaction between machine and the components, high accessibility in complex features, good aesthetic quality in welding or cutting areas, and easily automated procedure [14]. Additionally, lasers can cut a wide range of materials, from metals to plastics, in several industrial applications [15]. Melting or vaporization of the material can be accomplished via melt shearing or vaporization cutting using a laser. It helps achieve high surface quality by adjusting laser settings to get a small amount of surface roughness (SR), a minimum heat-affected zone (HAZ), and increased material utilization [16]. Many factors are effective in the laser cutting procedure. For example, a top edge (or taper geometry) is generated as the laser beam moves across the cutting surface [17]. Laser power (LP), frequency, scanning speed (SS), spot diameter, and stand-off distance, are also effective in the laser cutting process which requires optimization before starting the process [18].

Over the past few years, post-processing laser-based techniques on 3D-printed samples have been investigated to find out their influence on SR and integrity of polymer [19]. Researchers have used laser treatment to improve the surface quality or to cut the 3D-printed specimens accordingly [20]. Kechagias et al. [21] evaluated and adjusted CO_2 laser settings using a complete factorial design approach on 3D-printed polylactic acid (PLA) parts. It was found that this technique improved the SR values, which were between 1 and 6.2 μm. Also, build orientation was studied and it showed that both vertical and horizontal directions are effective in the laser cutting process. Results indicated the laser cutting procedure is effective in terms of enhancing surface integrity. Yilbas [22] investigated a law technique for kerf width (KW). Both the LP and the KW had direct alignment with each other. By increasing part thickness, KW increased as well while SS decreased accordingly. Also, Karimzad Ghavidel et al. [23] found a combination of low LP and high SS on low-density polyethylene (LDPE) and polystyrene (PS) decreased the area of HAZ. Furthermore, the material's SR and tensile strength are directly related to each other. Besides, Davim et al. [24] discovered that by reducing the LP, the HAZ depth was reduced while SR increased accordingly. Average surface roughness (R_a) was below 1 μm and 0.37 mm was achieved for HAZ in the CO_2 laser cutting process.

Moreover, Madić et al. [25] implemented useful tools, namely, Taguchi and response surface methodology (RSM), to find out the effects of LP in laser cutting and achieve accurate results. Also, Kurt et al. [26] observed polyoxymethylene (POM) and polytetrafluoroethylene (PTFE) had the same average roughness (0.4~1.4 μm) and shape accuracy errors in laser cutting while they had different properties. The assigning parameters in this study were plate thickness of 3 mm, 0.033, 0.083 and 0.133 mm/s of SS, 600, 900 and 1200 W of LP, and 2.5, 4.5, and 6.5 bar of gas pressure. Moradi et al. [27] used DOE and perceived 1.19 mm/s SS, 0.53 mm focal plane position (FPP), and 36.49 W LP in laser cutting to achieve the best quality. However, by changing the FPP, the kerf taper was increased. Eltawahni et al. [28] implemented analysis of variance (ANOVA) in Box–Behnken design and laser cutting process and found that 1436~1450 W LP, 700~704.76 mm/min SS, and −6.31 to −6.23 mm focal position were the optimal parameters to achieve the highest quality. Also, Vishnulal et al. [29] investigated laser cutting parameters and vibrational frequency in the workpiece to enhance cut quality in material removal rate of polymethyl methacrylate (PMMA), polycarbonate (PC), and polypropelyne (PP). Results indicated cutting areas improved when low frequency was varied from 12 to 24 Hz accordingly. Also, LP had a direct effect on cut quality up to a particular point, and then progressively decreased. Besides, Banerjee et al. [30] made a comparison of fluoroelastomers (FKM), polyamide 6 (PA6), and thermoplastic elastomers (TPEs) in laser cutting. Results showed TPE had less melted volume compared to the other two materials. According to the results, TPE's HAZ and RMS roughness were significantly less than those of PA6. The HAZ for PA6 was 700 μm, whereas the HAZ for TPE at 40 W LP was 230 μm. Kechagias et al. [31] developed a feedforward and back-propagation neural network (FFBP–NN) model to predict kerf characteristics in CO_2 laser cutting. The model was able to predict with better production times and smaller kerf angles. Results indicated strong interactions between the SS and stand-off distance were observed, and the parameter values that optimized the kerf angle resulted in positive values close to zero degrees were the 7 mm stand-off distance, 8 mm/s SS, and 97.5 W LP. The stand-off distance is the dominant parameter for the upper kerf width and kerf angle, while the SS is the most significant parameter for the middle and down kerf widths. These works show that CO_2 laser cutting as a post-processing technique is highly effective in enhancing the surface quality and integrity of products.

Besides the effectiveness of CO_2 laser cutting as a post-processing technique, there are factors in FFF procedure that affect the surface quality of printed products [32]. Vanaei et al. [33] investigated the optimization method on FFF by considering the speed and temperature of the 3D-printed nozzle on PLA sheets. The results showed the model can predict the layer adhesion and optimal printing speed and nozzle temperature. Van et al. [34] studied the extrusion parameters of FFF on PET material. This study aimed to enhance the stability of plastics by controlling the 3D-printing parameters. The FFF printing settings were adjusted to Ultimaker 3's printing temperature of 250 °C. It was also demonstrated that the combination of printing and build plate temperature, as well as fan cooling, had a significant influence on the level of crystallinity and, therefore, the mechanical characteristics of the printed components. Zhang et al. [35] investigated the effects of heat penetration on the thin sheets by FFF, in which PLA was selected as a filament. In this study, the layer was limited to 3 mm at a maximum rate because the thermal process could be monitored better in this case. Osswald et al. [36] investigated the effects of FFF parameters such as angle of nozzle, force, sink temperature, and speed control on polymer melting by a 3D printer. This study compared the results from experiments and models, showing that the model can effectively depict the melting process. Findings demonstrated with increasing inner nozzle tip angle, the melting rate drops. Along with this, as the filament force is raised from 20 to 100 N, the projected melt film thickness fluctuates between 80 and 35 μm.

Moreover, Medina-Sanchez et al. [37] investigated the building time of the FFF process on kinematics parameters on the printer, such as the speed of the nozzle. In this study, the proposed model accurately estimated the building time of specimens, and the error rate was below 9%. Chaidas et al. [38] examined how the nozzle temperature and layer thickness affect the quality of the surface and the dimensional accuracy of wood flour PLA using ANOVA. Results showed layer thickness had a significant effect on surface quality while by changing the nozzle temperature the surface quality slightly changed. This means that the layer thickness and nozzle temperature are effective on surface quality and accuracy in the printing procedure. Lalegani et al. [39] found out that the mechanical characteristics of 3D-printed PLA using computer-aided design (CAD) and FFF and their surface quality were directly impacted by the infill pattern and density. The results showed that the surface quality of the CAD specimens was marginally better. The surface quality of the grid and concentric designs was greatest, whereas the zigzag pattern performed poorly due to its subpar design and weak adherence. Burke et al. [40] investigated the printing orientation, nozzle diameter, and infill percentage (IP) of

3D-printed PLA using DOE. Results showed 5% infill percentage, flat orientation, and 0.2 mm nozzle diameter together resulting in the lowest surface roughness of 12.4 μm (0.2 mm). It can be seen the printing parameters are effective in terms of surface quality and dimensional accuracy. Hence, both CO_2 parameters and printing parameters are effective in producing products.

Despite a wide range of post-processing techniques on 3D-printed products, no research work has been done on laser cutting effects on curves and angles. It reveals that further experimentation is required to determine the feasibility of effectively integrating laser cutting into 3D-printed workpieces. Thus, in this research work, the surface quality of cone-shaped 3D-printed PLA parts made by the FFF process is investigated for the first time. A laser cutting machine is used to cut the printed sample with various parameters to study its effects on surface integrity. The present study evaluates extruder temperature and infill density in FFF process, followed by LP and SS in the laser cutting process. Also, the novelty of this study is the top edge and conical shape of the printed samples are the critical points due to the quality of the laser cutting effects in this area. Controlling these defects to have a high-quality cutting process is crucial. DOE methodology and ANOVA are implemented to analyse data and enhance the accuracy of obtained results in both FFF and laser cutting. The average SR of the cut in the post-processing technique and the geometry of the resulting top edge are chosen as surface quality criteria. By controlling the 3D printers and laser parameters, we can design a proper approach to decrease the rate of defects and increase post-processing capability. Also, this study helps to find the efficiency of the laser cutting quality on the top edge and the roughness of the printed samples through the layers after 3D printing by FFF (Fig. 1).

2. 3D printing process

FFF printed block PLA samples with a cone-shaped hole in the middle of them. Ultimaker S3 machine with two extruders printed square cubes with a size of 30 × 30 × 10 mm^3 in order to be laser cut from the middle of cone-shaped holes. All samples were printed in the same condition with constant parameters generated by Cura software. Black PLA filament (Ultimaker, Utrecht, Netherlands) was used in this study and the property of the material is provided in Table 1. The constant parameters were layer thickness of 0.15 mm, 0° build orientation, bed temperature of 60 °C, grid infill pattern, 45° raster angle and no support structure. However, extruder temperature and infill density were the only factors that were changed to find out the surface quality after the laser cut. By considering the 0.15 mm for the layer thickness, five layers on top and five layers on the bottom are printed accordingly.

Table 1
The material properties of Ultimaker PLA.

Feature	Value
Full name	Polylactic acid (PLA)
Melting temperature	151 °C
Crystallinity	37%
Chemical formula	$(C_3H_4O_2)_n$
High hardness	79 Shore D
Tensile modulus	2.7~16 GPa
Diameter	2.85 mm

Fig. 2 depicts the schematic of the sample and the area in which roughness is considered for the 3D roughness scanning. The values of extruder temperature and infill density are shown in Table 2. The extruder diameter was set to 0.4 mm to achieve reliable quality after the printing procedure. Fig. 3 shows the recorded cross-section layer pattern of the cones after printing using 10× magnification, which shows the sample layers were printed uniformly. In the roughness diagrams, the value of roughness in cross-section areas was measured to find out the effects of nozzle temperature and infill percentage. Both parameters are the most effective parameters in FFF process based on literature reviews, so here tried to show the effect of each parameter on the roughness quality. The nozzle temperature parameter is the temperature adjusted on the nozzle to melt the material during the 3D printing process and IP is defined as a kind of density when the 3D printer deposit material on the build plate [5]. The depth value was recorded between −40 μm and 40 μm and the path length was up to 4 μm. It is vital to have a smooth and uniform surface in these areas to avoid shrinkage and cracks in joining and welding sections [40,41]. Usually, due to the layer-by-layer binding in the 3D printing procedure, a stair step defect occurs, which has a great influence on the wall contacts. The mentioned defects are dependent on accuracy, geometric shape, process parameters, environmental impact, and material [42,43].

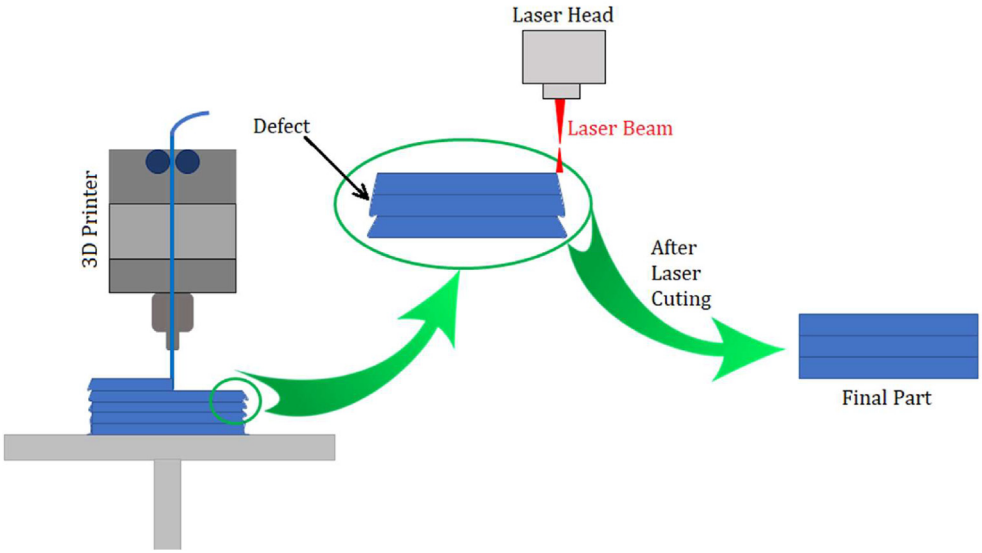

Fig. 1. Schematic of FFF polylactic acid and laser cutting process.

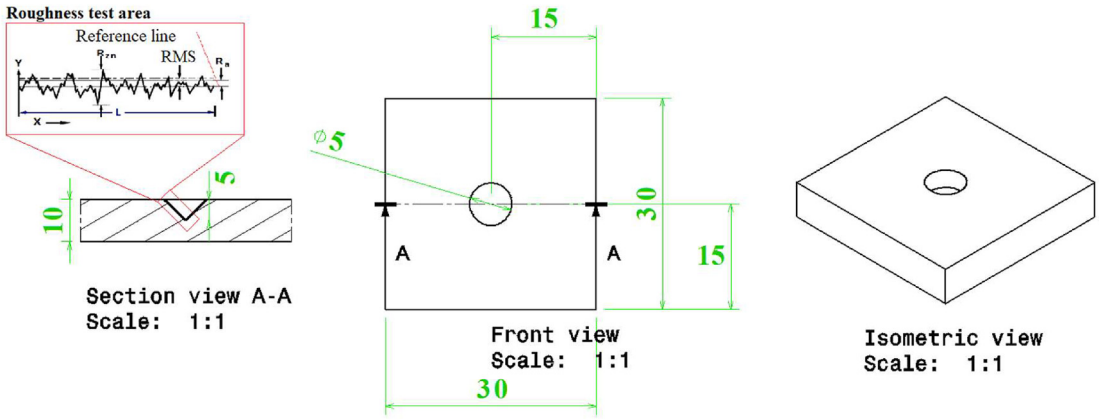

Fig. 2. The schematic of the sample and roughness area.

Table 2
Input and output parameters in the FFF process.

No.	Input		Output
	Infill percentage (%)	Extruder temperature (°C)	Roughness (μm)
#1	50	190	4.313
#2	30	250	11.957
#3	30	220	5.6
#4	10	250	2.644
#5	50	220	6.451
#6	30	220	4.834
#7	50	250	6.245
#8	30	220	5.011
#9	10	190	3.794
#10	30	220	5.016
#11	10	220	2.254
#12	30	190	2.151
#13	30	220	4.313

2.1. Surface roughness of 3D-printed samples

In Table 3, the values and the effects of 3D printer input parameters on roughness are examined with ANOVA by Design Expert V12. In this analysis, the interaction effects of different parameters in the DOE are also evaluated. A cubic model was selected and the effects of input parameters on each other were analyzed accordingly. The interaction between infill percentage and extruder temperature is crucial because by understanding the effects of each parameter on another one, we can find the proper parameters simultaneously.

The following regression Eqs. (1) and (2) show how to solve DOE numerically and the coefficient of each parameter's effect. In Eq. (1), the target is decreasing the roughness, so for achieving this goal, infill percentage and extruder temperature are considered the input parameters to have comprehensive effects of quadratic interaction of parameters on the roughness. The equation used coded factors to make predictions of the responses for the given levels accordingly. By default, the highest levels of the factors were coded as +1 and the lowest levels were coded as −1. The coded equation was useful to identify the relative impact of the factors by comparing the coefficients.

$$(Roughness)^1 = +4.13 + 2.74\ Infill\ Percentage + 5.11\ Extruder\ Temperature + 0.6783\ Infill\ Percentage \times Extruder\ Temperature - 1.21\ Infill\ Percentage^2 + 1.25\ Extruder\ Temperature^2 \quad (1)$$

The actual factors equation was used to make predictions for the response of the given levels of each factor. Here, the levels should be specified with the original units for each factor. This equation was not useful to determine the relative impact of each factor. The reason was that the coefficients were scaled to accommodate the units of each factor, and the intercept was not at the center of the design space.

$$(Roughness)^1 = 187.3691 - 8.7529\ Infill\ Percentage - 1.4215\ Extruder\ Temperature + 0.085364\ Infill\ Percentage \times Extruder\ Temperature + 0.087452\ Infill\ Percentage^2 + 0.002183\ Extruder\ Temperature^2 \quad (2)$$

Moreover, Fig. 4 provides information on the software prediction diagrams with real values, surface procedure, parameter effect interaction, and contour plot. Fig. 4(a) shows the measured outputs for roughness and estimates the outputs. The output results were close to the sloping line in both analyzers. It can be concluded that the software prediction was significantly in alignment with the actual results. Fig. 4(b) shows the response procedure diagram for surface roughness and ET and IP were considered as variable parameters. The 3D printer device had both parameters modifiable and choosing between the IP and ET ranges were flexible in this study. It is shown that by increasing the percentage of solidity and temperature of the extruder, the value of surface roughness increases in the vertical area of the cone and sample [26]. This phenomenon was because PLA creates a porous structure after melting through the nozzle. Also, transverse placement was low with high infill percentage and high temperature. Besides, this phenomenon caused non-uniformity of the printed layers on top of each other and reduced the roughness. Meanwhile, Fig. 4(c) shows the effects of the extruder temperature and infill percentage parameters. In this case, it was found that as the extruder temperature increased, the value of roughness also increased simultaneously. In fact, increasing the temperature caused instability in the printed layers. As a result, the percentage of overlap increased due to the melting of solidified layers, which made the whole surface uneven. At high temperatures, the molten material had enough time to absorb the oxygen in the air, which created porosity in the surface that increased the roughness, so by controlling the input parameters the rate of ununiform areas decrease significantly [26]. Also, Fig. 4(c) illustrates a contour plot of Fig. 4(d) in the *X* and *Z* coordinate plane, which shows the effective parameters in creating a more uniform surface texture in the cavity. According to the roughness diagrams of the printed cone, some roughness peaks were changed sharply. The reason is that by changing the direction of the printer nozzle and adding a bit of delay in this area, the extra filament was melted here, and some rocky particles were generated. Thus, after measuring the surface roughness by Alicona (IF-SensorR25, Alicona

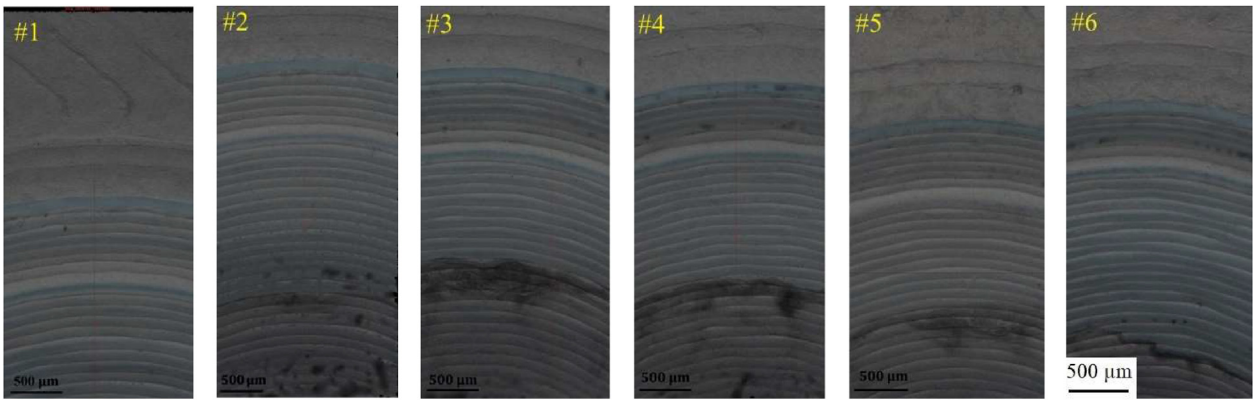

Fig. 3. Layers in the cross section of samples #1 to #6 after 3D scanning by Alicona device.

Table 3
ANOVA table of roughness.

Source	Sum of squares	df	Mean square	F–value	p–value	
Model	71.84	7	10.26	12.23	0.0070	Significant
A—Infill percentage	8.81	1	8.81	10.50	0.0230	
B—Extruder temperature	48.08	1	48.08	57.29	0.0006	
AB	2.37	1	2.37	2.83	0.0034	
A^2	7.66	1	7.66	9.13	0.0294	
B^2	2.96	1	2.96	3.53	0.0090	
Residual	4.20	5	0.8392			
Lack of fit	3.35	1	3.35	15.75	0.0166	Significant
Pure error	0.8497	4	0.2124			
Cor total	76.04	12				

Co., Australia), the output diagram shows a nonuniform surface in these sections.

2.2. Optimization of 3D printing samples

This section optimizes the input parameters of 3D-printed samples with a conical hole. Table 4 provides information on the importance of parameters in the DOE analysis. All input and output parameters had the highest influence, with a value of 3, which was the highest degree of importance in the research. The upper and lower limit constraints for each input and output parameter are shown in Table 4 as well. One of the main goals of Table 4 is elucidating the effective parameters and importance rate of the 3D printing operation, so here is tried to put importance three for IP and ET because both input parameters are highly effective in the 3D printing process [44]. Also, the input parameters were in range, but the roughness was considered as a low amount for the goal section of the DOE because by controlling the IP and ET in the effective range, it is possible to print samples with less roughness [45]. Moreover, Table 5 gives information on the optimal input parameters, and the predicted and actual output values of this study. The results indicated that the DOE was able to find the optimal parameters to achieve a relatively uniform surface in the conical region. Additionally, the desirability was recommended on three shapes and if this factor tends to one, the predicted amounts of output can be close to the real situation [46]. Also, the range of parameters for the optimum condition in Table 5 for IP and ET were calculated at 30%~45% and 200~216 °C, respectively.

Meanwhile, Fig. 5 shows the areas of optimal values. The yellow areas illustrate the ability of the FFF process and optimal parameters to print conical holes to achieve a better surface texture. Also, the grey area is a region where the parameters may not significantly affect the process in terms of output achievements. On the other hand, the parameters located in this area are not aligned with the best results of the experiment [47]. The interaction areas in Fig. 5 are very important because by selecting the parameters in yellow parts, the quality of the surface is better and the roughness decreases in these areas. This axis was selected based on the input parameters of the 3D printing process, so the software indicates optimum areas for the process by comparing the real and predicted amount of the optimum parameters. The rate of error on actual and predicted output for roughness was below 10%. Based on previous studies [2,9,14,23,32], this rate could be considered a reasonable rate for the accuracy of an experimental and numerical model of 3D printing.

3. Laser cutting

After the 3D printing procedure, the products sometimes need post-processing, such as drilling, cutting, welding, and sandblasting [48]. In this section, the effect and quality of the laser cutting on the top edge of the cutting zone were investigated. The laser cutting of printed specimens was examined to evaluate the top edge in these specimens. The aim of using the same technique for optimization was to save time and reach a better quality of post-processing which may satisfy RSM in this study. The laser cutting process is a vital procedure as a post-processing stage to eliminate defect areas or modify errors in surface texture after the printing procedure. In this research, a CO_2 laser with a maximum power of 1 kW was used to cut 3D-printed samples. The range of SS was from 1 mm/s to 5 mm/s. Fig. 6 shows a schematic of the laser cutting process and the sample cut after the process.

The cutting process in this research was done by using the DOE. In the initial design of the experiments, a total of 13 3D-printed samples were laser cut. LP and SS were considered as input

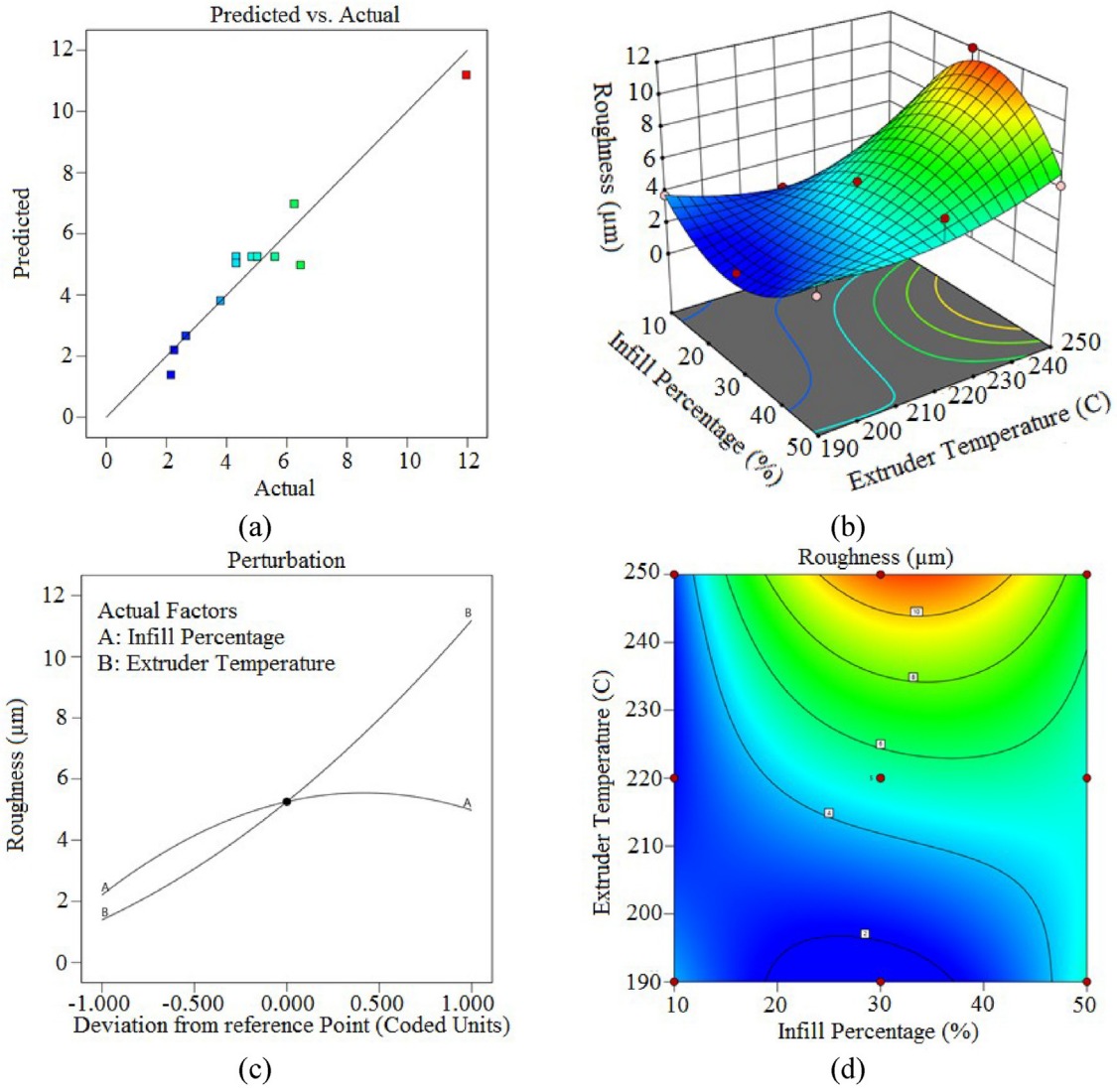

Fig. 4. Roughness response surface method diagrams of (a) predicted vs. actual results (b) response surface diagram for extruder temperature and infill percentage (c) perturbation plot and (d) contour plot.

Table 4
Constraints of 3D printing samples.

Name	Goal	Lower limit	Upper limit	Lower weight	Upper weight	Importance
Infill percentage (%)	is in range	10	50	1	1	3
Extruder temperature (°C)	is in range	190	250	1	1	3
Roughness	Low	2.151	11.957	1	1	3

parameters, while the top edge was chosen as the output parameter. The reason to select these input and output parameters is that changing the SS and LP is more effective for considering the top-edge behavior after the cutting process [25]. Thus, by changing just SS and LP, it is possible to save time to reach optimum parameters for the CO_2 cutting. The optimally generated prototype top edge was measured by ImageJ. Table 6 shows the values of input and output parameters for the cutting process. Also, Fig. 7 illustrates samples 1 to 13 after laser cutting operations.

3.1. Top edge

Table 7 depicts the ANOVA of the laser cutting process. The cubic model was used for detecting of interaction between the laser input parameters.

The final equation in terms of coded factors is shown in Eqs. (3) and (4). The coded factors equations were used to make predictions of the response for given levels of each factor. By default, the highest levels of the factors were coded as +1 and the lowest levels

Table 5
Optimum solutions for 3D printing of cones.

	Input			Output	
Number	Infill percentage (%)	Extruder temperature (°C)	Desirability		Roughness
1	35	216	1	Predicted	4.987
				Actual	5.112
2	30	215	0.9985	Predicted	5.178
				Actual	5.077
3	45	200	0.9723	Predicted	4.875
				Actual	4.863

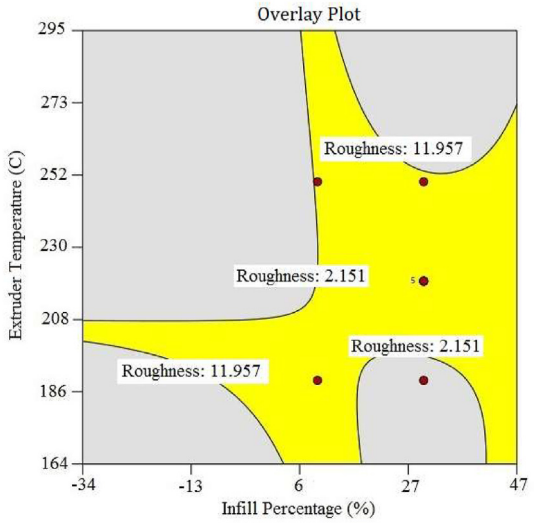

Fig. 5. Contour plot of highly effective area for the lowest roughness 3D-printed cones.

Table 6
Input and output parameters in the laser cutting process.

No.	Input		Output
	LP (W)	SS (mm/s)	Top edge (μm)
#1	300	3	302
#2	400	3	341
#3	400	3	335
#4	400	5	310
#5	400	3	337
#6	500	1	391
#7	400	3	336
#8	300	5	275
#9	500	3	373
#10	500	5	347
#11	400	1	354
#12	300	1	315
#13	400	3	339

were coded as −1. The coded equation was useful for identifying the relative impact of the factors by comparing the factor coefficients:

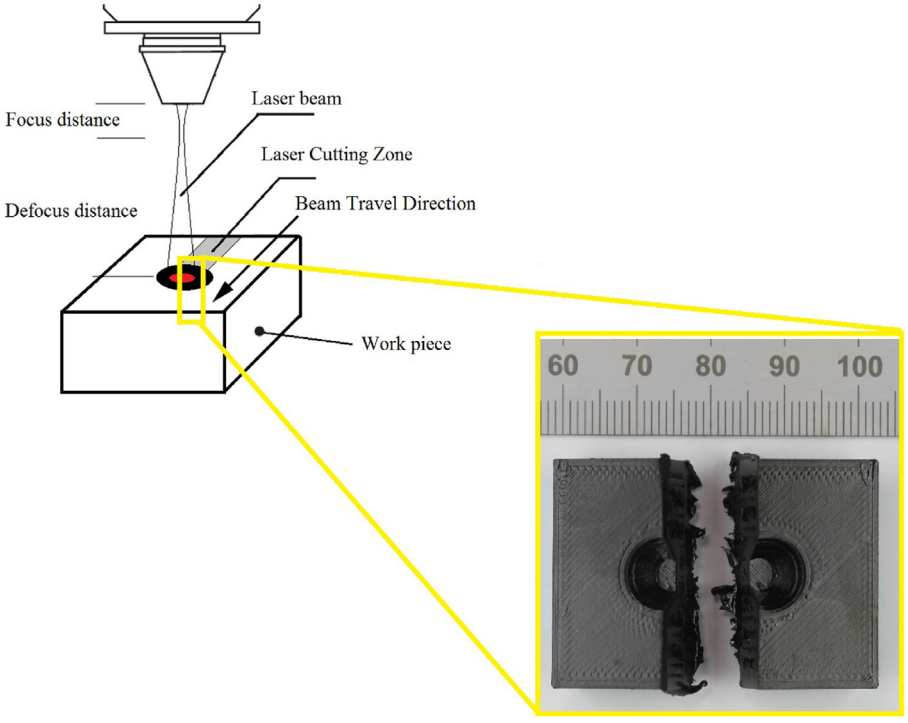

Fig. 6. Laser cutting process of 3D-printed sample.

Fig. 7. 3D-printed sample after laser cutting for samples #1 to #13.

Table 7
ANOVA model of top edge value.

Source	Sum of squares	df	Mean square	F–value	p–value	
Model	10832.79	7	1547.54	333.42	<0.0001	Significant
C—LP	2520.50	1	2520.50	543.05	<0.0001	
D—SS	968.00	1	968.00	208.56	<0.0001	
CD	4.00	1	4.00	0.8618	0.0058	
C^2	0.0074	1	0.0074	0.0016	0.0197	
D^2	85.13	1	85.13	18.34	0.0078	
Residual	23.21	5	4.64			
Lack of fit	2.69	1	2.69	12.78	0.02741	Significant
Pure error	23.20	4	5.80			
Cor total	10856.00	12				

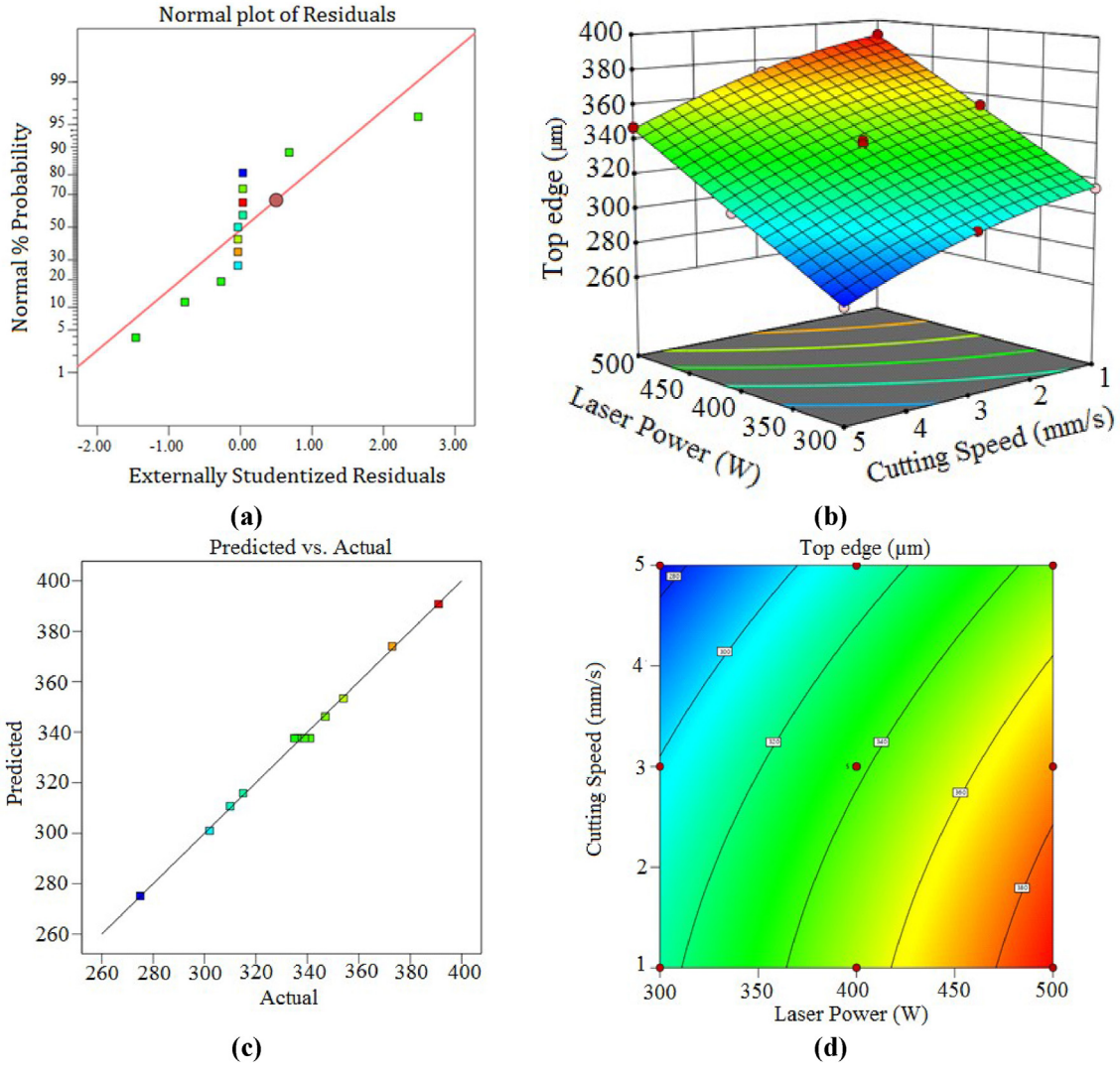

Fig. 8. Top edge diagrams of (a) normal plot of residuals (b) response surface plot of LP and SS (c) predicted vs. actual plot (d) contour plot of LP and SS.

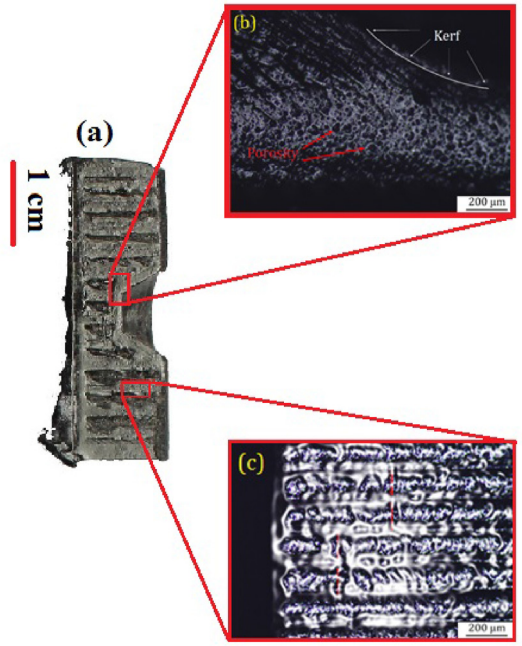

Fig. 9. Cross section (a) sample #4 after laser cutting process, (b) the cone and porosity on the cutting area, (c) boundaries of the layers on the melting points after 3D printing.

$$Top\ edge = +223.47 + 27.87\ Laser\ Power - 11.78\ Cutting\ speed - 1.0000\ Laser\ Power \times Cutting\ speed - 0.02475\ Laser\ Power^2 - 4.71\ Cutting\ speed^2 \quad (3)$$

The equation in terms of actual factors was used to make predictions about the response to given levels of each factor. Here, the levels were specified in the original units for each factor. Equation (4) should not be used to determine the relative impact of each factor because the coefficients are scaled to accommodate the units of each factor and the intercept is not at the center of the design space.

$$Top\ edge = +115.112587 + 0.748365\ Laser\ Power + 7.8574215\ Cutting\ speed - 0.186325\ Laser\ Power \times Cutting\ speed - 0.0742154\ Laser\ Power^2 - 3.853624\ Cutting\ speed^2 \quad (4)$$

Fig. 8 shows the DOE of top edge that was analyzed by the RSM method and plotted with the design expert program. Fig. 8(a) shows the normal plot of residuals, the percentage of scatter and residues in the DOE analysis. The oblique line is seen in this figure as an indicator of the stability of the data scatter. The more inclined the data was to this line, the more reliable the output data was for optimization. Fig. 8(b) provides information on the interaction of the laser input parameters, including the speed and power, at the same time on the top edge scale. By increasing the power and decreasing the speed of laser scanning, the interaction of the laser beam with the surface of the printed samples increased, which led to an increase in the inlet heat to the surface [31,32]. As the input heat of the laser increased, more amount of the material was melted. As a result, the value of top edge increased as well. Fig. 8(c) shows the graph of actual and predicted results. This graph shows a detailed analysis of software output data which is largely equal to the actual measured values. From the input data. Also, Fig. 8(d) illustrates the contour plot in the 2D view. Results provide details that in the red areas, the value of inlet heat and top edge is maximum, and the blue area shows the lowest value of top edge.

Fig. 9(a) shows the defects and top edge changes of the printed layers (No. 4) after laser cutting process. The printed layers had overlapped due to the high temperature of the nozzle during the printing procedure. The generated heat by the laser on the PLA surface was sublimated, and the material was converted from solid to vapor [15]. The cutting operation interacted with the ambient air and created porosity in the mentioned area (see Fig. 9(b)). Although this process completely cut the printed samples, the surface of the sample was not damaged or affected by the laser in areas that were far from the heat-affected areas. Also, by considering Fig. 9, it is clear that some layers are mixed and the material blended because the laser's heat was higher than the polymer's melting point, and heating in the affected area created a pool in which some of the material mixed properly. By considering Fig. 9(b) and (c), it is found that layers after the laser cutting process were mixed properly because the boundaries of the layers disappeared after the cutting process.

3.2. Optimization of the laser cutting process

The laser-cutting process was optimized by considering the input and output parameters, which led to a numerical solution for the optimal parameters. Table 8 shows the importance of specified input and output parameters by assigning a coefficient to each. In this study, all three input and output parameters had the highest coefficient with the degree of importance three because each of these parameters is critical for the process. Based on Table 6, the lower and upper rates of LP and SS were adjusted, so these three and the weight in the regression method considered one to have the least squares in the residuals [5]. Table 9 also shows the predicted and actual values for all three optimal samples. Since the error coefficient in all three optimal samples in top edge values was less than 15%, DOE analysis can be considered a reliable method [28]. The coded value of parameters was converted to actual data and shown based on the input and output parameters. Also, comparing the predicted and actual data shows a better map of using the DOE for top edge cutting which can be modified by the RSM [40].

Table 9
Optimum solutions for the laser cutting process.

	Input			Output	
Number	LP (W)	SS (mm/s)	Desirability		Top edge (µm)
1	302	1.9	1	Predicted	280
				Actual	297
2	300	2	0.9856	Predicted	301
				Actual	295
3	300	1	0.9235	Predicted	310
				Actual	307

Table 8
Constraints of CO_2 laser cutting samples.

Name	Goal	Lower limit	Upper limit	Lower weight	Upper weight	Importance
LP (W)	is in range	300	500	1	1	3
SS (mm/s)	is in range	1	5	1	1	3
Top edge (µm)	Low	275	391	1	1	3

4. Conclusion

The results of the current study have demonstrated the viability of using CO_2 laser cutting to reduce the surface roughness of FFF components. The impacts of laser cutting parameters on 3D-printed surfaces with cone shapes were discussed. The surface roughness of printed samples which were printed using the DOE method was investigated based on infill percentage and extruder temperature. By taking into account the suitable amount of infill percentage and extruder temperature, the lowest roughness value was reported to be 2.151 μm, which had a uniform surface texture. The findings showed that the value of the top edge rose to 307 μm with increasing LP and decreasing SS. This occurred as a result of the laser beam's intense engagement with the material's surface, which eventually increased the amount of heat applied to the surface. In the operation of laser treatment, the material is removed, followed by a change in the dimension that must be taken into consideration while developing components. The proposed method can be applied to other types of thermoplastic with slippery surfaces. By creating larger layers and then using a laser-cutting process to restore the surface's roughness to an acceptable level, the productivity of the FFF process can be boosted.

Conflicts of interest

The authors declare that there is no conflicts of interest.

References

[1] M. Lalegani Dezaki, M.K.A. Mohd Ariffin, S. Hatami, An overview of fused deposition modelling (FDM): research, development and process optimisation, Rapid Prototyp. J. 27 (2021) 562–582.
[2] Ch Abeykoon, S. Pimpisut, F. Anura, Optimization of fused deposition modeling parameters for improved PLA and ABS 3D printed structures, Int. J. Lightweight Mater. Manuf. 3 (2020) 284–297.
[3] S.C. Daminabo, S. Goel, S.A. Grammatikos, H.Y. Nezhad, V.K. Thakur, Fused deposition modeling-based additive manufacturing (3D printing): techniques for polymer material systems, Mater. Today Chem. 16 (2020), 100248.
[4] K.A. Al-Ghamdi, Sustainable FDM additive manufacturing of ABS components with emphasis on energy minimized and time efficient lightweight construction, Int. J. Lightweight Mater. Manuf. 2 (4) (2019) 338–345.
[5] S. Ashen, B.B. Kanbur, Y. Zhou, F. Duan, Thermal and mechanical assessments of the 3D-printed conformal cooling channels: computational analysis and multi-objective optimization, J. Mater. Eng. Perform. 29 (2020) 8261–8270.
[6] L. Le, M.A. Rabsatt, H. Eisazadeh, M. Torabizadeh, Reducing print time while minimizing loss in mechanical properties in consumer FDM parts, Int. J. Lightweight Mater. Manuf. 5 (2) (2022) 197–212.
[7] Z. Lu, O.I. Ayeni, X. Yang, H.Y. Park, Y.G. Jung, J. Zhang, Microstructure and phase analysis of 3D-printed components using bronze metal filament, J. Mater. Eng. Perform. 29 (2020) 1650–1656.
[8] A. Jaisingh Sheoran, H. Kumar, Fused Deposition modeling process parameters optimization and effect on mechanical properties and part quality: review and reflection on present research, Mater. Today Proc. 21 (2020) 1659–1672.
[9] M. Pérez, G. Medina-Sánchez, A. García-Collado, M. Gupta, D. Carou, Surface quality enhancement of fused deposition modeling (FDM) printed samples based on the selection of critical printing parameters, Materials 11 (2018).
[10] N.N. Kumbhar, A. v Mulay, Post processing methods used to improve surface finish of products which are manufactured by additive manufacturing technologies: a review, J. Inst. Eng.: Series C 99 (2018) 481–487.
[11] M.H. Ali, S. Kurokawa, E. Shehab, M. Mukhtarkhanov, Development of a Large-scale multi-extrusion FDM printer, and its challenges, Int. J. Lightweight Mater. Manuf. 6 (2023) 198–213.
[12] J.S. Chohan, R. Singh, Pre and post processing techniques to improve surface characteristics of FFF parts: a state of art review and future applications, Rapid Prototyp. J. 23 (2017) 495–513.
[13] R.T. Mushtaq, Y. Wang, M. Rehman, A.M. Khan, M. Mia, State-Of-the-Art and trends in CO_2 laser cutting of polymeric materials—a review, Materials 13 (2020).
[14] M.H. El-Hofy, H. El-Hofy, Laser beam machining of carbon fiber reinforced composites: a review, Int. J. Adv. Manuf. Technol. 101 (2019) 2965–2975.
[15] M. Barletta, A. Gisario, Laser sealing of PLA-based compostable coffee capsules, Opt. Laser. Technol. 133 (2021), 106557.
[16] P. Stavropoulos, A. Koutsomichalis, N. Vaxevanidis, Laser-based manufacturing processes for aerospace applications, in: I.R.M. Association (Ed.), Materials Science and Engineering: Concepts, Methodologies, Tools, and Applications, IGI Global, Hershey, PA, USA, 2017, pp. 374–391.
[17] N. Ahmed, S. Darwish, A.M. Alahmari, Laser ablation and laser-hybrid ablation processes: a review, Mater. Manuf. Process. 31 (2016) 1121–1142.
[18] R. Dewil, P. Vansteenwegen, D. Cattrysse, A review of cutting path algorithms for laser cutters, Int. J. Adv. Manuf. Technol. 87 (2016) 1865–1884.
[19] V.K. Tiwary, A. P, V.R. Malik, An overview on joining/welding as post-processing technique to circumvent the build volume limitation of an FFF-3D printer, Rapid Prototyp. J. 27 (2021) 808–821.
[20] F. Caiazzo, F. Curcio, G. Daurelio, F.M.C. Minutolo, Laser cutting of different polymeric plastics (PE, PP and PC) by a CO_2 laser beam, J. Mater. Process. Technol. 159 (2005) 279–285.
[21] J.D. Kechagias, K. Ninikas, M. Petousis, N. Vidakis, N. Vaxevanidis, An investigation of surface quality characteristics of 3D printed PLA plates cut by CO2 laser using experimental design, Mater. Manuf. Process. 36 (2021) 1544–1553.
[22] B.S. Yilbas, Laser cutting quality assessment and thermal efficiency analysis, J. Mater. Process. Technol. 155–156 (2004) 2106–2115.
[23] A. Karimzad Ghavidel, M. Shabgard, H. Biglari, Microscopic and mechanical properties of semi-crystalline and amorphous polymeric parts produced by laser cutting, J. Appl. Polym. Sci. 133 (2016).
[24] J.P. Davim, C. Oliveira, N. Barricas, M. Conceição, Evaluation of cutting quality of PMMA using CO2 lasers, Int. J. Adv. Manuf. Technol. 35 (2008).
[25] M. Madić, M. Radovanović, M. Manić, M. Trajanović, Optimization of CO_2 laser cutting process using taguchi and dual response surface methodology, Tribol. Ind. 36 (2014) 236.
[26] M. Kurt, Y. Kaynak, E. Bagci, H. Demirer, M. Kurt, Dimensional analyses and surface quality of the laser cutting process for engineering plastics, Int. J. Adv. Manuf. Technol. 41 (2009) 259–267.
[27] M. Moradi, M. Karami Moghadam, M. Shamsborhan, M. Bodaghi, H. Falavandi, Post-processing of FDM 3D-printed polylactic acid parts by laser beam cutting, Polymers 12 (2020).
[28] H.A. Eltawahni, A.G. Olabi, K.Y. Benyounis, Effect of process parameters and optimization of CO_2 laser cutting of ultra high-performance polyethylene, Mater. Des. 31 (2010) 4029–4038.
[29] R.K. Vishnulal, P. Govindan, M.P. Vipindas, Laser machining of polymer materials – experimental investigations - process challenges and strategies, in: S.C. Satapathy, K.S. Raju, K. Molugaram, A. Krishnaiah, G.A. Tsihrintzis (Eds.), International Conference on Emerging Trends in Engineering (ICETE), Springer International Publishing, Cham, 2020, pp. 653–661.
[30] S.S. Banerjee, A. K, Bhowmick, experimental study on the CO_2 laser cutting of novel polyamide 6/fluoroelastomer thermoplastic elastomeric blends, Rubber Chem. Technol. 88 (2015) 125–137.
[31] J.D. Kechagias, K. Ninikas, P. Stavropoulos, K. Salonitis, A generalised approach on kerf geometry prediction during CO_2 laser cut of PMMA thin plates using neural networks, Lasers Manuf. Mater. Process. 8 (3) (2021) 372–393.
[32] J. Kechagias, D. Chaidas, N. Vidakis, K. Salonitis, N.M. Vaxevanidis, Key parameters controlling surface quality and dimensional accuracy: a critical review of FFF process, Mater. Manuf. Process. (2022) 1–22.
[33] H.R. Vanaei, S. Khelladi, M. Deligant, M. Shirinbayan, A. Tcharkhtchi, Numerical prediction for temperature profile of parts manufactured using fused filament fabrication, J. Manuf. Process. 76 (2022) 548–558.
[34] B. Van de Voorde, A. Katalagarianakis, S. Huysman, A. Toncheva, J.M. Raquez, I. Duretek, C. Holzer, L. Cardon, K.V. Bernaerts, D. Van Hemelrijck, L. Pyl, Effect of extrusion and fused filament fabrication processing parameters of recycled poly (ethylene terephthalate) on the crystallinity and mechanical properties, Addit. Manuf. 50 (2022), 102518.
[35] J. Zhang, B. Van Hooreweder, E. Ferraris, T4F3: temperature for fused filament fabrication, Prog. Addit. Manuf. (2022) 1–21.
[36] T.A. Osswald, J. Puentes, J. Kattinger, Fused filament fabrication melting model, Addit. Manuf. 22 (2018) 51–59.
[37] G. Medina-Sanchez, R. Dorado-Vicente, E. Torres-Jiménez, R. López-García, Build time estimation for fused filament fabrication via average printing speed, Materials 12 (23) (2019) 3982.
[38] D. Chaidas, J.D. Kechagias, An investigation of PLA/W parts quality fabricated by FFF, Mater. Manuf. Process. 37 (5) (2022) 582–590.
[39] M. Lalegani Dezaki, M.K.A.M. Ariffin, A. Serjouei, A. Zolfagharian, S. Hatami, M. Bodaghi, Influence of infill patterns generated by CAD and FDM 3D printer on surface roughness and tensile strength properties, Appl. Sci. 11 (16) (2021) 7272.
[40] C. Burke, A. Dalal, A. Abukhalaf, R. Noorani, Effects of process parameter variation on the surface roughness of polylactic acid (PLA) materials using design of experiments (DOE), vol. 897, no. 1, in: IOP Conference Series: materials Science and Engineering, IOP Publishing, 2020, July, 012003.
[41] X. Sun, J. Zhou, Q. Wang, J. Shi, H. Wang, PVA fibre reinforced high-strength cementitious composite for 3D printing: mechanical properties and durability, Addit. Manuf. 49 (2022), 102500.
[42] E. Ferretti, M. Moretti, A. Chiusoli, L. Naldoni, F. De Fabritiis, M. Visonà, Rice-husk shredding as a means of increasing the long-term mechanical properties of earthen mixtures for 3D printing, Materials 15 (3) (2022) 743.

[43] L. Ma, Q. Zhang, Z. Jia, C. Liu, Z. Deng, Y. Zhang, Effect of drying environment on mechanical properties, internal RH and pore structure of 3D printed concrete, Constr. Build. Mater. 315 (2022), 125731.
[44] A. Kottasamy, M. Samykano, K. Kadirgama, M. Rahman, M.M. Noor, Experimental investigation and prediction model for mechanical properties of copper-reinforced polylactic acid composites (Cu-PLA) using FDM-based 3D printing technique, Int. J. Adv. Manuf. Technol. (2022) 1–22.
[45] A. Tayeb, J.B. Le Cam, B. Loez, 3D printing of soft thermoplastic elastomers: effect of the deposit angle on mechanical and thermo-mechanical properties, Mech. Mater. 165 (2022), 104155.
[46] Y. He, H. Xie, Y. Ge, Y. Lin, Z. Yao, B. Wang, M. Jin, J. Liu, X. Chen, Y. Sun, Laser cutting technologies and corresponding pollution control strategy, Processes 10 (4) (2022) 732.
[47] T. Qin, Z. Zhong, H. Jiao, L. Zhou, Y. Huang, Y. Long, Experimental study on gas-assisted laser cutting carbon fiber reinforced plastics, Int. J. Adv. Manuf. Technol. 119 (9) (2022) 6361–6370.
[48] E. Haddadi, M. Moradi, A.K. Ghavidel, A.K. Ghavidel, S. Meiabadi, Experimental and parametric evaluation of cut quality characteristics in CO_2 laser cutting of polystyrene, Optik 184 (2019) 103–114.